Available online at www.sciencedirect.com
ScienceDirect
Proceedings of the Combustion Institute 33 (2011) 1957–1965
Proceedings of the Combustion Institute
www.elsevier.com/locate/proci

Combustion of alane and aluminum with water for hydrogen and thermal energy generation

Terrence L. Connell Jr. [a,*], Grant A. Risha [a], Richard A. Yetter [a], Gregory Young [b], Dilip S. Sundaram [c], Vigor Yang [c]

[a] Department of Mechanical and Nuclear Engineering, The Pennsylvania State University, USA
[b] RDT&E Department, Naval Surface Warfare Center – Indian Head Division, USA
[c] School of Aerospace Engineering, Georgia Institute of Technology, USA

Available online 16 October 2010

Abstract

The combustion of alane and aluminum with water in its frozen state has been studied experimentally and theoretically. Both nano and micron-sized particles are considered over a broad range of pressure. The linear burning rate and chemical efficiency are obtained using a constant-pressure strand burner and constant-volume cell, respectively. The effect of replacing nano-Al particles by micron-sized Al and alane particles are examined systematically with the additive mass fraction up to 25%. The equivalence ratio is fixed at 0.943. The pressure dependence of the burning rate follows the power law, $r_b = aP^n$, with n ranging from 0.41 to 0.51 for all the materials considered. The burning rate decreases with increasing alane concentration, whereas it remains approximately constant with cases containing only Al particles. The chemical efficiency ranged from 32% to 83%, depending on the mixture composition and pressure. Thermo-chemical analyses are conducted to provide insight into underlying causes of the decreased burning rate of the alanized compositions. A theoretical model is also developed to explore the detailed flame structure and burning properties. Reasonably good agreement is achieved with experimental observations.

Keywords: Aluminum hydride; Hydrogen generation; Nano particles; Combustion; Chemical efficiency

1. Introduction

The aluminum–water reaction has been the subject of scientific research during the past 50 years due to its ability to liberate large amounts of energy and green exhaust products [1–4]. Ingentio and Bruno [5] suggested that aluminum/steam reactions can possibly produce a specific impulse greater than 300 s. Thus, coupled with the emergence of nano-sized particles, researchers have been examining Al and water mixtures for propulsion, power generation, and hydrogen production due to its efficient two-component configuration [6–9]. Considerable efforts have recently been made to investigate the combustion of Al–water mixtures in both the liquid and frozen phases [10–14]. These studies have shown high conversion efficiencies in constant-volume experiments and very high burning rates with nanometer sized Al particles. Results also revealed that micron-sized particles are difficult to ignite and to maintain a self propagating reaction. The hydrogen

* Corresponding author. Address: 105 Research Building East, State College, PA 16802, USA. Fax: +1 814 865 3389.
E-mail address: tlc252@psu.edu (T.L. Connell).

1540-7489/$ - see front matter © 2010 The Combustion Institute. Published by Elsevier Inc. All rights reserved.
doi:10.1016/j.proci.2010.07.088

Nomenclature

C_p	constant-pressure specific heat
d_p	particle diameter
h	enthalpy
k	ratio of burning velocity to thermal diffusivity
L	thickness of reaction zone
S_L	burning rate relative to unburned mixture
T	temperature
t	thickness of preheat zone
U	burning rate relative to mixture at relevant interface
x	density weighted coordinate, $\int_0^{x'} (\rho/\rho_{\mathrm{mix},5})\, dx'$
x'	physical coordinate of the system
y	normalized coordinate, $x/U_5\ \tau_0$

Subscripts

0	prior to ignition
deh	dehydrogenation
f–g	liquid–vapor phase change
i	index for preheat zone; particle class
melt	melting
mix,*i*	mixture in the *i*th zone
R	dehydrogenation reaction
si,*i*	ignition of particle of class *i*
s–l	solid–liquid phase change
u	unburned
vap	vaporization

Greek symbols

α	thermal diffusivity
ζ	normalized density, $\rho_{\mathrm{mix},i}/\rho_{\mathrm{mean}}$
θ	normalized temperature, T/T_u
κ	normalized diffusivity, $U_i^2\tau_0/\alpha_{\mathrm{mix},i}$
λ	thermal conductivity
μ	normalized heat release
ρ	density
τ_0	reference time scale, $\tau_{b0,1} + \tau_{b0,2}$
τ_b	burning time of aluminum particle
χ	normalized particle diameter, d_p/d_{p0}

yield from a mixture of unpassivated Al and water is approximately 5.6% on a mass basis. However, all Al particles have a passivating oxide layer, which prevents oxidation of the Al at ambient conditions. A significant portion of nano-sized Al particles is aluminum oxide (e.g., a 50-nm Al particle contains only 68% by mass pure Al [7]). Consequently, the hydrogen yields are much lower than the theoretical value for pure Al particles. Two approaches for minimizing the initial mass of aluminum oxide, and thus increasing the gravimetric yield of hydrogen, are to replace portions of the nanometer Al with micron Al or introduce other ingredients rich in hydrogen [15,16].

Aluminum hydride, or alane, has been broadly used in many energetic materials due to its high hydrogen storage capacity (theoretically, 10.1% by weight) [17–24]. Alane is a covalently bonded hydride which often appears in a polymeric form $(AlH_3)_n$ and has at least seven known non-solvated forms. The most stable polymorph is α-AlH_3 [19,25,26]. Alane decomposition or dehydrogenation (an endothermic process) has been found to be dependent on particle size [20], doping stimulants, form, structure [20], and heating rates [20,27]. Young et al. [27] found that micron-sized alane ignites in air at temperatures similar to those of nano-Al particles. Decomposition temperatures have been observed to be as low as 60 °C at low heating rates with doping, and as high as 900 °C at extremely high heating rates [20,27]. In shock tube studies, Bazyn et al. [28] determined that once the hydrogen in alane has been released, the remaining Al burns on time scales equivalent to similarly sized Al particles.

Micron-sized Al particles typically contain less than 1% alumina by mass. Recently, Connell et al. [29] studied the effect of adding micron-sized (2 and 5 μm) Al particles on the burning rate of a baseline mixture containing 80-nm Al particles and water. The equivalence ratio was fixed at 0.943. The loading of micron-sized particles ranged from 0% to 80% of the Al particle mass, increasing the active Al content from ~74.5% to 91%. The linear burning rate was not noticeably affected until the micron particle substitution exceeded 20% of the active fuel mass, at which point the burning rate decreased. The mixture always remained ignitable with sustained flame propagation, regardless of the loading fraction of micron-sized particles.

The present work attempts to study the effect of micron-sized alane and Al particles on the combustion and hydrogen generation of the nano-Al and water based reactive mixture. Both the reaction propagation rate and combustion efficiency were determined. The alane particles were characterized with thermal and microscopy analyses. In addition, a chemical equilibrium analysis was performed and a theoretical model of the flame propagation process was developed.

2. Chemical equilibrium analysis

In order to determine the effects of micron-sized alane and Al as additives to nAl/ice

mixtures, and to identify viable reactive mixture compositions, thermo-chemical calculations were performed using the NASA chemical equilibrium with applications (CEA) Program [30]. The pressure was 7 MPa (1015 psia). The active Al content of the nano-Al was 74.5% by mass with the balance being alumina, while the micron-sized Al and alane were considered to be 100% pure fuel. Figure 1a–c exhibit the results of the equilibrium calculations. The equivalence ratio, ϕ, of the mixtures was held constant at 0.943. The baseline case considered contained 80-nm Al particles and frozen water (ice). A small addition of alane exerts a significant impact on the equilibrium flame temperature and product composition. The alanized fuel shows a 10% increase in the specific impulse ($\sim[T_{\text{prod}}/\text{MW}_{\text{prod}}]^{0.5}$) and a 5% reduction in the flame temperature relative to the baseline case. The former can be attributed to the substantial decrease in the overall molecular weight of the product species. Figure 1b shows that the addition of alane increases the mole fraction of hydrogen generated, while simultaneously reducing the mole fraction of alumina. Such a reduction of alumina also mitigates the two-phase flow losses in the exhaust nozzle of a propulsion device. The fuel containing micron-sized Al exhibits a modest improvement in the specific impulse (~2%), which can be attributed to the reduction of inert alumina, when the nano-sized Al is replaced by the micron-sized Al. Figure 1c shows the flame temperatures and I_{sp} for the baseline nano-Al/ice mixture compared to fuels containing 20% micron-sized Al or alane as a function of the equivalence ratio. Clearly, the alanized formulation leads to the highest performance, while maintaining the lowest flame temperature under most conditions. All three formulations demonstrate a temperature plateau under fuel rich conditions corresponding approximately to the melting temperature of aluminum oxide (~2300 K). However, the highest temperature and I_{sp} always occur near the stoichiometric condition.

3. Experimental approach

The experimental study involves measurements of the linear burning rate and hydrogen yield over a range of pressures using a windowed constant-pressure strand burner and a constant-volume cell, respectively.

3.1. Sample preparation

The reactive mixtures under investigation were comprised of 80-nm (procured from Nanotechnologies, Inc.), 20-μm Al particles (Sigma–Aldrich), and 20-μm Al hydride particles combined with de-ionized distilled water. The 80-nm "as received" nano particles were passivated for 96–120 h in air, reducing the active Al content from 77–79% to ~74.5%, to prevent the occurrence of low-temperature reactions [10]. Both the alane and micron Al particles were assumed to be 100% active, since the alumina content of the 20-μm Al is small and the alane is believed to be absent of any oxide. De-ionized water was purchased from Electron Microscopy Sciences (Reagent A.C.S Cat#22800-01), reporting a maximum of 0.01 ppm silicate, 0.01 ppm heavy metals, and 10 ppm of residue (after removal from packaging, due to evaporation). Proper amounts of 80-nm Al particles combined with either 20-μm Al or alane particles were premixed using a Resodyne LabRAM® acoustic mixer to break up agglomerates and produce a homogenous fuel composition prior to oxidizer addition. A detailed description of the passivation technique and mixing process is given in Ref. [10]. The mixture was filled into quartz sample tubes (10-mm OD, 8-mm ID) and then frozen at −35 °C. Recorded packing densities for the 100% 80-nm composition with $\phi = 0.943$ were 1.60 ± 0.03 g/cm^3, while increasing the mass fractions of 20-μm Al and alane particles showed decreasing packing densities, ranging from 1.51 ± 0.03 g/cm^3 for 25% 20-μm Al particle addition to 1.44 ± 0.03 g/cm^3 for 25% alane particle addition.

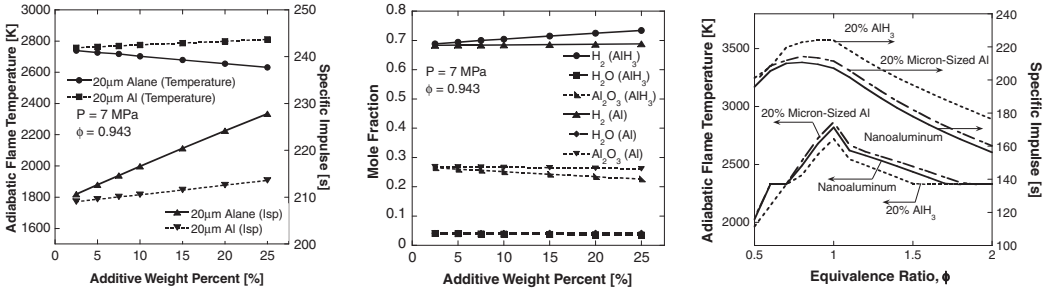

Fig. 1. Adiabatic flame temperature, specific impulse, and product mole fractions as a function of fuel additive weight percentage.

3.2. Particle characterization and thermal analysis

High resolution scanning electron microscopy (SEM) images of the fuel particles are shown in Fig. 2. The 80-nm Al particles exhibit spherical characteristics in contrast to the rhombohedral-shaped alane. The 20-μm Al particles have a wider particle distribution compared to the other particles. Thermo-gravimetric analysis (TGA) and differential scanning calorimetry (DSC) experiments were performed on separate samples of alane and Al particles, as well as mixtures of the particles, to quantify the low-temperature thermal characteristics in an argon atmosphere with trace amounts of oxygen. The TGA/DSC results (Fig. 3) indicate that the alane powder begins decomposition at approximately 150 °C, which is consistent with published data [18–20]. Furthermore, the mass lost during the process showed a 9.6% reduction, accounting for the hydrogen lost, which is close to the theoretical hydrogen mass content of 10.1%. Further heating of the alane (or Al) particle exhibited an endotherm in the DSC profile at approximately 660 °C indicating melting of the Al.

3.3. Combustion experiments

Strand burner experiments were conducted at nearly constant-pressure to obtain linear and mass burning rates of various reactive mixtures, as functions of both pressure and mixture composition. Details of the system specifications and ignition procedures can be found in Refs. [9,10]. Argon gas was used as a pressurant to achieve the desired chamber pressure. Sample ignition was achieved via a 28 gauge nichrome hot-wire and NOSOL 363 (classical double based gun propellant) booster charge. The chamber operating pressures ranged between 0.86 and 15 MPa (125–2175 psia). A Setra pressure transducer provided static monitoring of the chamber pressure, and the pressure data were recorded at 500 Hz. The combustion event was photographically recorded using a Sony digital video camera. The linear burning rate was correlated using a conventional St. Robert's power law fit, which is given in Eq. (1) as,

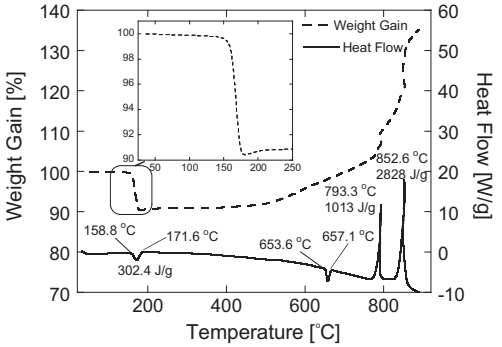

Fig. 3. TGA and DSC results of neat alane in an argon (with trace amounts of oxygen) atmosphere.

$$r_b[\mathrm{cm/s}] = A(P[\mathrm{MPa}])^n \tag{1}$$

where A is a constant pre-exponential coefficient and n is the pressure exponent [31].

Constant-volume chemical efficiency [32] was measured using a 181 cm^3 constant-volume vessel, to determine the effects of pressure and mixture composition on the hydrogen yield. The operational pressure ranged up to 69 MPa (10,015 psia). Quartz tubes (3.2 cm × 1 cm) containing ~2 g of reactive mixture ($\phi = 0.943$) were placed onto a carriage and positioned into the center of the vessel. Argon gas was flowed into the chamber, allowing continuous flushing of the gas in the chamber and purging of the entrapped air, until the required initial pressure was achieved. Ignition was achieved via a coiled 28 gauge nichrome filament (without the NOSOL booster) embedded into the reactive mixture surface prior to freezing. The output signals from the dynamic pressure transducer were recorded at 5 kHz during the experiment. After completion of the burning, the trapped gas products in the chamber were sampled using a calibrated gas chromatograph (Agilent 3000 Micro GC) at 153 kPa (22.2 psia) to determine the concentration of molecular

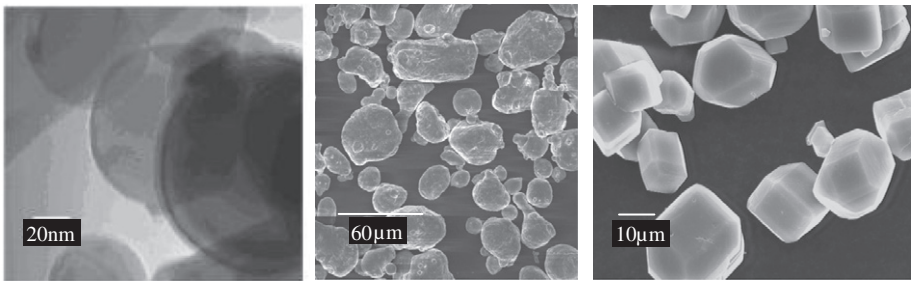

(a) 80-nm aluminum (b) 20-μm aluminum (c) 20-μm Alane

Fig. 2. (a) TEM and (b and c) SEM images of particles considered [17].

hydrogen. The chemical efficiency was obtained by relating the measured hydrogen concentration to the theoretical maximum value based on the stoichiometry and reactant composition.

4. Model development

A theoretical model was developed to understand the flame propagation behavior of the mixture. Details of the model are presented in Ref. [33]. Steady-state and one-dimensional approximations are invoked. The entire region of interest is divided into six zones: (1) Al/AlH_3-ice preheat zone; (2) Al/AlH_3-liquid water preheat zone; (3) Al/AlH_3-steam preheat zone; (4) Al/H_2-steam preheat zone; (5) nano-sized particle reaction zone; and (6) micron-sized particle reaction zone, as shown schematically in Fig. 4. The alane particles are assumed to dehydrogenate prior to ignition [28]. The governing equations and corresponding boundary conditions are presented below. The analytical solutions for the energy equation in the preheat zones are readily derivable and are not presented here. The mixture density and the thermal conductivity are calculated based on the volume fractions of the species, while the mixture specific heat is calculated based on the mass fractions. Thermo-physical properties are calculated at a mean temperature in each zone.

Al/AlH_3-ice preheat zone (I):

$$\rho_{\mathrm{mix},5}U_5C_{\mathrm{pmix},1}\frac{dT}{dx'}=\lambda_{\mathrm{mix},1}\frac{d^2T}{dx'^2}$$
$$\begin{cases} x'\to-\infty: T\to T_u, \\ x'=-(t_1+t_2+t_3): T=T_{\mathrm{melt}}; \end{cases} \quad (2)$$

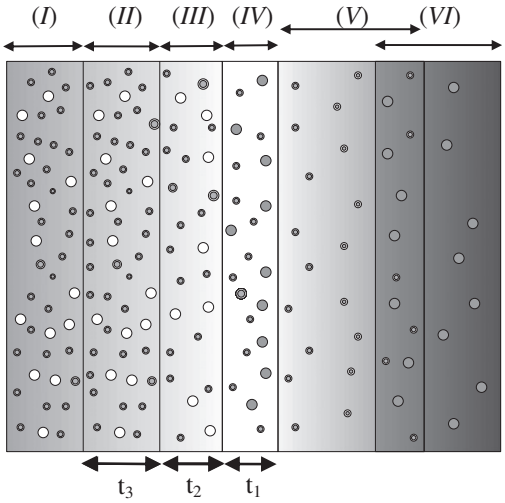

Fig. 4. Multi-zone framework used in the analysis (alane depicted by large white circles, nAl by small gray circles, and μAl by large gray circles).

Al/AlH_3-liquid water preheat zone (II):

$$\rho_{\mathrm{mix},5}U_5C_{\mathrm{pmix},2}\frac{dT}{dx'}=\lambda_{\mathrm{mix},2}\frac{d^2T}{dx'^2};$$
$$\begin{cases} x'=-(t_1+t_2+t_3): \lambda_{\mathrm{mix},2}\frac{dT}{dx'}=\lambda_{\mathrm{mix},1}\frac{dT}{dx'}+\rho_{\mathrm{H_2O}}h_{s-l}S_L, \\ x'=-(t_1+t_2): T=T_{\mathrm{vap}}; \end{cases} \quad (3)$$

Al/AlH_3-steam preheat zone (III):

$$\rho_{\mathrm{mix},5}U_5C_{\mathrm{pmix},3}\frac{dT}{dx'}=\lambda_{\mathrm{mix},3}\frac{d^2T}{dx'^2};$$
$$\begin{cases} x'=-(t_1+t_2): \lambda_{\mathrm{mix},3}\frac{dT}{dx'}=\lambda_{\mathrm{mix},2}\frac{dT}{dx'}+\rho_{\mathrm{H_2O}}h_{f-g}S_L, \\ x'=-t_1: T=T_{\mathrm{deh}}; \end{cases} \quad (4)$$

Al/H_2-steam preheat zone (IV):

$$\rho_{\mathrm{mix},5}U_5C_{\mathrm{pmix},4}\frac{dT}{dx'}=\lambda_{\mathrm{mix},4}\frac{d^2T}{dx'^2};$$
$$\begin{cases} x'=-t_1: \lambda_{\mathrm{mix},4}\frac{dT}{dx'}=\lambda_{\mathrm{mix},3}\frac{dT}{dx'}+\rho_{\mathrm{AlH_3}}h_rU_3, \\ x'=0: T=T_{\mathrm{si},1}; \end{cases} \quad (5)$$

Reaction zone (V, VI):

The present method extended the approach described in [34] to treat both mono-dispersed and bimodal mixtures as given by Eqs. (6) and (7) for the normalized temperature and particle diameter. The particle ignition temperature and burning time are required inputs [34]. The ignition temperature of 20 μm and 80 nm aluminum particles are taken as 1883 and 1165 K, respectively [34]. The single particle burning time correlation is taken from Ref. [34], while the pressure exponent is taken as a function of ambient temperature [35].

$$\frac{d^2\theta}{\mathrm{dy}^2}-\kappa^2\zeta\frac{d\theta}{\mathrm{dy}}=-\mu_1\kappa^2\zeta^2(\theta_{\mathrm{si},1}-1)\frac{\tau_0}{\tau_{b,1}}-\eta\mu_2\kappa^2\zeta^2(\theta_{\mathrm{si},2}-1)\frac{\tau_0}{\tau_{b,2}};$$
$$\eta=\begin{cases} 0; T<T_{\mathrm{si},2} \\ 1; T\geqslant T_{\mathrm{si},2} \end{cases}; \begin{cases} y=0: \theta=\theta_{\mathrm{si},1}, \lambda_{\mathrm{mix},5}\frac{d\theta}{\mathrm{dy}}\Big|_{0+}=\lambda_{\mathrm{mix},4}\frac{d\theta}{\mathrm{dy}}\Big|_{0-}, \\ y\to L: \frac{d\theta}{\mathrm{dy}}\to 0. \end{cases} \quad (6)$$

The variation of the particle diameter can be obtained from its burning time. In the present analysis, an average particle mass consumption rate is employed. The mass consumption rate is the initial particle mass divided by the burning time calculated based on its initial particle size and local temperature.

$$\frac{d\chi_1}{\mathrm{dy}}=-\frac{1}{3\chi_1^2}\frac{\tau_0}{\tau_{b,1}};$$
$$\frac{d\chi_2}{\mathrm{dy}}=-\frac{\eta}{3\chi_2^2}\frac{\tau_0}{\tau_{b,2}}; \begin{cases} y=0: \chi_i=1, \\ y\to L: \chi_i\to 0. \end{cases} \quad (7)$$

In Eq. (7), the subscript i refers to the particle class ($i=1$, 2 for nano-sized and micron-sized particles, respectively).

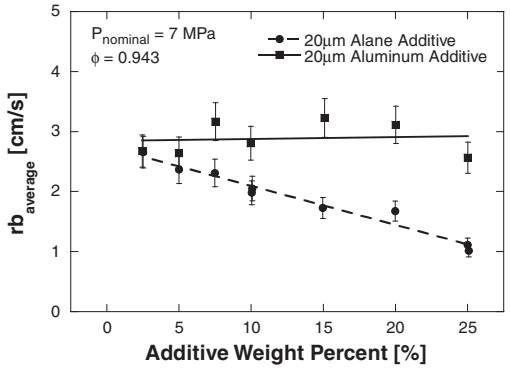

Fig. 5. Effect of additive weight percentage on linear burning rate at a nominal pressure of 7 MPa.

5. Results and discussion

Figure 5 shows the linear burning rate of the reactive mixtures as a function of additive weight percent at a nominal pressure of 7 MPa. Mixtures consisting of nano and micron-sized Al particles have a relatively constant burning rate (~2.8 cm/s) over the range of conditions tested. Connell et al. [29] have shown that the linear burning rate (at 7 MPa) held approximately constant for up to 40% addition of 2-μm aluminum particles and 20% for 5-μm particles, beyond which the linear burning rates began to decrease. In contrast, the burning rate of a mixture containing alane particles decreased from 2.6 to 1 cm/s as the amount of alane increased. This phenomenon can be attributed to the lower flame temperature caused by the endothermic decomposition of alane.

The effect of pressure on the burning rate is given in Fig. 6a and b. For all the cases considered here, the burning rate increases with increasing pressure. However, the situation is reversed with alane concentration. The addition of alane particles reduce the burning rate, while 20 μm Al compositions (with the same weight percentages) are similar to the 80-nm baseline, achieving a slightly faster burning rate for the highest pressure. A similar trend was found by Connell et al. [29] using 2 versus 20 μm Al particles. Although ignition of the mixture with 75% 80-nm Al and 25% alane was achieved at 3.55 MPa (515 psia), the burning rate could not be attained due to the diminished luminosity of the combustion front. The low luminosity is another indication of decreasing reaction temperatures with alane addition. The respective parameters in the St. Robert's burning law for each formulation are provided in the figures.

Constant-pressure efficiency tests were conducted by varying the additive weight percentage at a nominal pressure of 7 MPa (Fig. 7). The average chemical efficiency for the baseline propellant was ~72%. Chemical efficiencies of approximately 80% were presented by Risha et al. [7] for a similar 80-nm aluminum and water composition, over a similar range of pressures. The combustion efficiency for the frozen baseline composition should be slightly lower due to additional loss associated with the phase change from ice to water. The

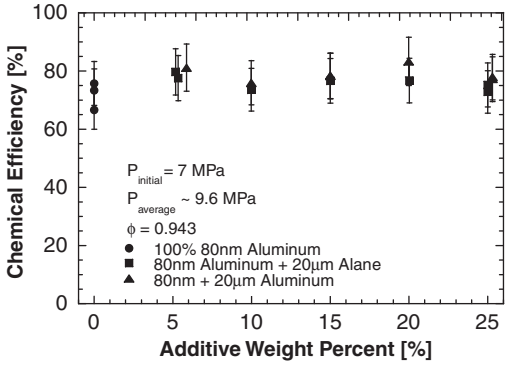

Fig. 7. Chemical efficiencies of various mixtures at an initial pressure of 7 MPa.

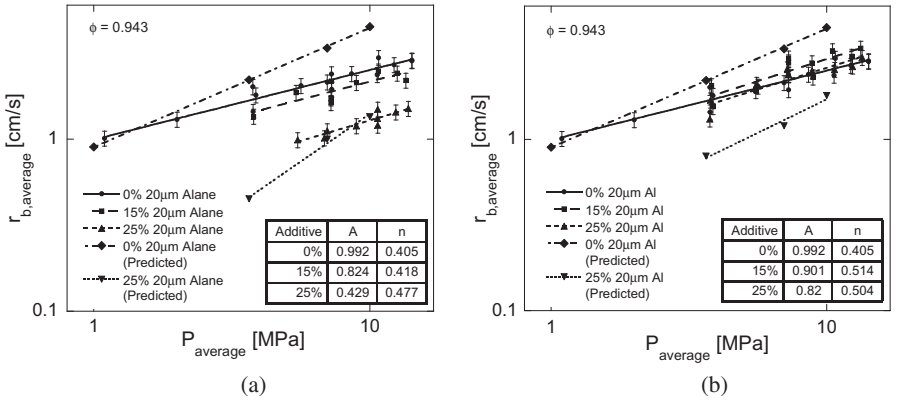

(a) (b)

Fig. 6. Linear regression rate results for mixtures containing: (a) alane and (b) 20-μm Al.

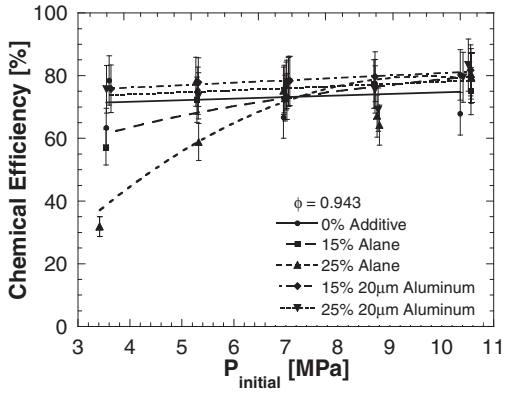

Fig. 8. Chemical efficiencies for various mixtures and different initial pressures.

bimodal propellant compositions with either alane or micron-sized Al showed a slight increase in chemical efficiency compared to the baseline results. The results, however, remained approximately constant with increasing additive substitution. Efficiencies for the 80-nm and 20-μm Al cases appear to be slightly higher than those with similar compositions containing alane particles. In the constant-volume experiments, the pressure increase (ΔP) during reaction for alane-loaded mixtures decreased from 5.5 to 4 MPa with increasing particle addition, while the pressure generated by the micron-sized Al composition was approximately constant (5.3–5.5 MPa).

Figure 8 shows the chemical efficiency for various initial pressures using the same mixture formulations as those in the strand burner experiments. The efficiency for the baseline mixture increased from 63% to 80%, when the pressure increased from 3.55 to 10.4 MPa (515–1515 psia). Increases in efficiency for bimodal compositions are also shown, with the most significant being with the 15% and 25% alane compositions, which increase from 60% and 32% respectively to ~80% at the highest pressure. The efficiencies for 80- and 20-μm Al particles were slightly elevated from the baseline, following a similar, linearly increasing trend. Connell et al. [29] indicated that with increasing active Al content, the reaction temperature increases, due to a reduced initial alumina concentration. Both the increased equivalence ratio and reduced alumina concentration resulted in a higher adiabatic combustion temperature, promoting formation of molten alumina and improving the reactivity of the composite fuel. The burning rate and chemical efficiency thus increased accordingly.

The predicted linear burning rates are also shown in Fig. 6a and b. The model predicts a thicker flame for the bimodal mixtures, because of the presence of two different reaction zones associated with nano and micron-sized particles. The longer burning time of larger particles leads to a wider reaction zone. The flame thickness predicted by the model is about 1 mm for the bimodal mixture and 0.1 mm for the baseline 80 nm particle mixture. The nano-Al particles start to burn first due to their lower ignition temperature, whereas the micron-sized particles remain relatively inert. In later stages of reaction, the energy released by the combustion of nano-aluminum particles is sufficient to ignite micron-sized particles. An overlapped flame configuration is observed.

As shown in Fig. 6, the burning rates of the bimodal aluminum mixtures are consistent with the baseline, with 15% 20 μm composition increasing from approximately 3% to 16% (0.05–0.5 cm/s) above the baseline, and the 25% 20 μm formulation lying directly on the baseline over the range of pressures tested. Burning rates of alane compositions are shown to decrease up to ~50% compared to the baseline with increasing alane weight percentage. This is not surprising considering that nano particles burn relatively faster than micron-sized particles and the adiabatic flame temperature decreases with the addition of alane. The higher flame temperatures of aluminum/ice mixtures help explain the observed decrease in the burning rate associated with the alanized formulation. Since the burning rate is dictated by the heat transfer from the flame zone to the condensed phase, such a lower flame temperature of the alanized composition contributes to the reduction in the burning rate. This behavior is consistent with the experimental observation in which the burning rate decreases with increasing alane content, whereas it remains nearly constant or even increases slightly with micron-sized aluminum. The theoretical results show reasonably good agreement with the experimental data. The treatment of multi-phase flow is simplified by employing a mixture model and assuming equilibrium between different phases. In addition, radiation heat transfer is neglected in the present analysis. Furthermore, accurate burning time data are not available for single nAl particles burning in a liquid water environment at high pressures. These assumptions are believed to be reasons for the disparity between experimental measurements and numerical predictions. Further improvement is warranted.

6. Conclusions

The combustion of Al/alane/ice reactive mixtures was characterized over a range of pressures and compositions. Thermo-chemical results show that small quantities of alane added to the baseline formulation can increase the specific impulse by ~10%, while reducing flame temperatures by ~5%. Furthermore, the presence of alane produces more hydrogen in the products, reducing the alumina mole fraction. The linear burning rate

and chemical efficiency are relatively unaffected by the substitution of 20-μm Al particles under constant-pressure conditions. The burning rate decreases with increasing alane addition, due to reduced adiabatic reaction temperature, although the chemical efficiency remains nearly constant.

The linear burning rates for all formulations considered increase with increasing pressure, and are correlated well using a power law. The pressure exponents for the baseline and 80-nm Al/alane cases were shown to be similar (ranging from 0.405 to 0.477), while the pre-exponential factor decreases from 0.992 to 0.429 with increasing additive weight percentage. The chemical efficiency increases with increasing pressure from approximately 32%, reaching a plateau around 80%. Compositions with 80-nm and 20-μm Al particles have similar pre-exponential values which are slightly lower than the value of the baseline case (decreasing from 0.992 to 0.82), and pressure exponents increase from 0.405 to 0.504. The chemical efficiency increases with increasing pressure from 72% to approximately 80%, and follows the same trend as the baseline composition.

The model predicts a thicker flame for bimodal mixtures compared with cases using mono-dispersed nano-Al particles, due to higher burning times inherent of micron-sized particles. The three mixtures considered exhibit similar pressure dependence of the burning rate. The replacement of 25% micron-sized Al particles for nano-Al results in a similar linear burning rate. Substitution of 20-μm alane (~25%) for micron-sized Al in the mixture indicates a decrease in burning rates compared to the baseline of approximately 1–1.4 cm/s (~50%) over the pressure range of interest, while maintaining the same increasing trend. The phenomenon can be attributed to the lower flame temperature resulting from the addition of alane.

Acknowledgements

The sponsorship by the Air Force Office of Scientific Research (AFOSR) and NASA for this program under Contract No. FA9550-07-1-0582 is greatly appreciated. The authors greatly appreciate Rob Uhlig, Bryan Sones, and Lynn Witherite at the Applied Research Laboratory of The Pennsylvania State University for providing the test cell facility for high-pressure strand experiments. Thanks are also due to Bohan Kuo for her assistance in setup and calibration of the Micro GC.

References

[1] L. Greiner, *ARS J.* 30 (1960) 1161–1163.
[2] L. Greiner, *Underwater Missile Propulsion*, Compass Publications Inc., Arlington, VA, 1962.
[3] V.G. Ivanov, O.V. Gavrilyuk, O.V. Glazkov, M.N. Safronov, *Combust. Explo. Shock Waves* 36 (2) (2000) 213–219.
[4] J.P. Foote, J.T. Lineberry, B.R. Thompson, B.C. Winkelman, Investigation of aluminum particle combustion for underwater applications, AIAA Paper, 1996-2086, 32nd AIAA/ASME/SAE/ASEE Joint Propulsion Conference, Orlando, FL, 1996.
[5] A. Ingenito, C. Bruno, *J. Propul. Power* 20 (6) (2004) 1056–1063.
[6] G.A. Risha, Y. Huang, R.A. Yetter, V. Yang, S.F. Son, B.C. Tappan, Combustion of aluminum particles with steam and liquid water, AIAA Aerospace Sciences Meeting and Exhibit, 9–12 January 2006, Reno, Nevada, AIAA 2006-1154.
[7] G.A. Risha, S.F. Son, R.A. Yetter, V. Yang, B.C. Tappan, *Proc. Combust. Inst.* 31 (2) (2007) 2029–2036.
[8] T.F. Miller, J.D. Herr, Green Rocket Propulsion by Reaction of Al and Mg Powders and Water, AIAA 2004-4037, 2004.
[9] J.L. Sabourin, G.A. Risha, R.A. Yetter, S.F. Son, B.C. Tappan, *Combust. Flame* 154 (3) (2008) 587–600.
[10] G.A. Risha, T.L. Connell Jr., R.A. Yetter, et al., Aluminum-ice (ALICE) propellants for hydrogen generation and propulsion, 45th AIAA/ASME/SAE/ASEE Joint Propulsion Conference and Exhibit, Denver, CO, AIAA Paper No. 2009-4877, August 2–5, 2009.
[11] H. Adirim, S. Poller, H. Schoyer, D. Muss, F. Caramelli, Advanced ELV propulsion solutions: cryogenic solid propellants, 39th AIAA/ASME/SAE/ASEE Joint Propulsion Conference and Exhibit, Huntsville, AL, AIAA Paper No. 2003-5209, July 20–23, 2003.
[12] R.E. Lo, H. Adirim, S. Poller, Cryogenic solid propulsion technology development status, 40th AIAA/ASME/SAE/ASEE Joint Propulsion Conference and Exhibit, Fort Lauderdale, FL, AIAA Paper No. 2004-3477, July 11–14, 2004.
[13] H. Adirim, R.E. Lo, N. Pilz, et al., Cryogenic solid propulsion technology development status, 41st AIAA/ASME/SAE/ASEE Joint Propulsion Conference and Exhibit, Tucson, AZ, AIAA Paper No. 2005-4093, July 10–13, 2005.
[14] H. Adirim, R.E. Lo, N. Pilz, et al., State-of-the-art in solid propulsion research, 42nd AIAA/ASME/SAE/ASEE Joint Propulsion Conference and Exhibit, Sacramento, CA, AIAA Paper No. 2006-4420, July 9–12, 2006.
[15] J.G. Lee, M. Weismiller, T.L. Connell, G.A. Risha, R.A. Yetter, Ammonia borane based-propellants, 44th AIAA/ASME/SAE/ASEE Joint Propulsion Conference and Exhibit, Hartford, CT, AIAA Paper No. 2008-5037.
[16] M. Diwan, D. Hanna, A. Varma, *Int. J. Hydrogen Energy* 35 (2010) 577–584.
[17] J. Graetz, J.J. Reilly, *J. Phys. Chem. B* 109 (47) (2005) 22181–22185.
[18] J. Graetz, J.J. Reilly, *J. Alloys Compd.* 424 (1–2) (2006) 262–265.
[19] J. Graetz, J.J. Reilly, J.G. Kulleck, R.C. Bowman, *J. Alloys Compd.* 446–447 (2007) 271–275.
[20] G. Sandrock, J. Reilly, J. Graetz, W.M. Zhou, J. Johnson, J. Wegrzyn, *Appl. Phys. A: Mater. Sci. Process.* 80 (4) (2005) 687–690.

[21] J.G.O. Ojwang, R.A. van Santen, G.J. Kramer, A.C.T. van Duin, W.A. Goddard, *J. Chem. Phys.* 131 (2009) 044501-1–044501-13.
[22] V. Weiser, N. Eisenreich, A. Koleczko, E. Roth, *Propellants Explos. Pyrotech.* 32 (3) (2007) 213–221.
[23] L.T. Deluca, L. Galfetti, F. Severini, et al., *Aerosp. Sci. Technol.* 11 (1) (2007) 18–25.
[24] G. Young, G.A. Risha, A.G. Miller, R.A. Glass, T.L. Connell, R.A. Yetter, *Int. J. Energ. Mater. Chem. Propul.*, submitted for publication.
[25] F.M. Brower, N.E. Matzek, P.F. Reigler, et al., *J. Am. Chem. Soc.* 98 (9) (1976) 2450–2453.
[26] M.A. Petrie, J.C. Bottaro, R.J. Schmitt, P.E. Penwell, D.C. Bomberger, Preparation of Aluminum Hydride Polymorphs, Particularly Stabilized α-AlH_3, US Patent No. US 6228,338.
[27] G. Young, N. Piekiel, S. Chowdhury, M.R. Zachariah, *Combust. Sci. Technol.*, submitted for publication.
[28] T. Bazyn, R. Eyer, H. Krier, N. Glumac, *J. Propul. Power* 20 (3) (2004) 427–431.
[29] T.L. Connell, G.A. Risha, R.A. Yetter, V. Yang, S.F. Son, *Int. J. Energ. Mater. Chem. Propul.*, submitted for publication.
[30] B.J. Mcbride, S. Gordon, Computer Program for Calculation of Complex Chemical Equilibrium Compositions and Applications, Reference Publication 1311, NASA, 1996.
[31] G.P. Sutton, O. Biblarz, *Rocket Propulsion Elements: An Introduction to the Engineering of Rockets*, sixth ed., John Wiley and Sons, Inc., 1992.
[32] G.A. Risha, J.L. Sabourin, V. Yang, R.A. Yetter, S.F. Son, B.C. Tappan, *Combust. Sci. Technol.* 180 (2008) 2127–2142.
[33] D.S. Sundaram, V. Yang, T.L. Connell, G.A. Risha, R.A. Yetter, G. Young, *Combust. Sci. Technol.*, submitted for publication.
[34] Y. Huang, G.A. Risha, V. Yang, R.A. Yetter, *Combust. Flame* 156 (1) (2009) 5–13.
[35] T. Bazyn, H. Krier, N. Glumac, *Combust. Flame* 145 (2006) 703–713.